Journal of Organometallic Chemistry 954–955 (2021) 122074

Contents lists available at ScienceDirect

Journal of Organometallic Chemistry

journal homepage: www.elsevier.com/locate/jorganchem

Synthesis, structure, spectral, redox properties and anti-cancer activity of Ruthenium(II) Arene complexes with substituted Triazole Ligands

Arabinda Muley[a], Kalai Selvan Karumban[a], Parth Gupta[b], Sadananda Kumbhakar[a], Bishnubasu Giri[a], Rajnikant Raut[b], Ashish Misra[b,*], Somnath Maji[a,*]

[a] Department of Chemistry, Indian Institute of Technology, Hyderabad, Kandi, Sangareddy 502284, Telangana, India
[b] Department of Biotechnology, Indian Institute of Technology, Hyderabad, Kandi, Sangareddy 502284, Telangana, India

ARTICLE INFO

Article history:
Received 15 July 2021
Revised 26 August 2021
Accepted 2 September 2021
Available online 8 September 2021

Keywords:
Redox-active ligand
Ruthenium-arene complexes
Electrochemistry
Crystal structures
Anticancer activity
In vitro cytotoxicity

ABSTRACT

Three versatile half-sandwich ruthenium(II) *p*-cymene complexes bearing substituted triazole ligands exhibit promising cancer cell growth inhibition activity towards A549 lung adenocarcinoma and MDA-MB-231 breast adenocarcinoma cells. In this context, the triazole based phthalimide protected new ligand (2-(3, 5-di(pyridin-2-yl)-4H-1,2,4-triazol-4-yl) isoindoline-1,3-dione) ($\mathbf{L^1}$) was prepared. Three ruthenium(II) *p*-cymene complexes [Ru(η^6-*p*-cymene)($\mathbf{L^1}$)Cl]Cl: [**1**]Cl, $\mathbf{L^1}$: (2-(3,5-di(pyridin-2-yl)-4H-1,2,4-triazol-4-yl)isoindoline-1,3-dione), [Ru(η^6-*p*-cymene)($\mathbf{L^2}$)Cl]Cl: [**2**]Cl and [Ru(η^6-*p*-cymene)($\mathbf{L^2}$)Cl](PF_6): [**2**](PF_6), $\mathbf{L^2}$ (2,2′-(4-(1H-pyrrol-1-yl)-4H-1,2,4-triazole-3,5-diyl) dipyridine) have been successfully synthesized and characterized by different spectral and analytical tools. Pyrrole protected substituted ruthenium complexes [**2**]Cl and [**2**](PF_6) have been successfully identified structurally by single-crystal X-ray diffraction studies and confirmed the successful anion exchange. The redox properties of the ligands and the targeted metal complexes have been carefully examined. Cellular staining, live-cell imaging and MTT assay have been performed for all the complexes. We have demonstrated that our synthesized ruthenium(II) *p*-cymene complexes are capable of inducing significant cytotoxicity in A549 lung cancer cell lines, with an IC_{50} values of 6.56 ± 0.31 μM, 4.74 ± 0.2 μM and 13.67 ± 0.64 μM and in MDA-MB-231 breast cancer cell lines with an IC_{50} values of 1.13 ± 0.046 μM, 0.36 ± 0.016 μM and 11.32 ± 0.49 μM for [**1**]Cl, [**2**]Cl and [**2**](PF_6) respectively.

1. Introduction

Cancer persists to be a major concern for humankind for long times and the pursuit of anticancer agents has an evolving and ever-growing history over the last few decades [1]. The increase of population density, industrialization and other environmental factors have directly contributed to the spike of cancer cases worldwide [2] demanding the scientific community to design and develop potent anticancer drugs with low toxicity and high selectivity and efficacy [3]. The major issues with the traditional cancer treatment approach, such as radiation therapy, chemotherapy, surgery, etc., lies in molecular oxygen dependency, biocompatibility, selectivity, expense, insufficient optimization protocols, etc., together with controlled clinical trials [4,5]. In this regard, chemotherapeutic agents based on platinum (cisplatin, carboplatin, oxaliplatin, etc.) have gained special attention over the years, but their severe side effects like nerve damage, nephrotoxicity and myelotoxicity have made them unsuitable for broader application [6]. Also, the acquired drug resistance of cisplatin and analogues remains a barrier towards its further improvement and clinical usage [7]. Optimization of these factors requires specific attention towards designing other metal-based cost-effective drugs for the development of anticancer agents [8].

However, ruthenium complexes could be promising alternatives due to their lower toxicity towards healthy cells in the biological environment [9–11]. Two major classes of ruthenium-based complexes have gained enormous attention in the pharmaceutical field. Primarily robust oxidation catalysts, ruthenium polypyridyls are also employed as anticancer drugs [12,13] and ruthenium arenes, with their half sandwich structures are highly suitable for *in vitro* studies [14–17]. Due to their structural identity, the distinct class of arene ruthenium(II) complexes are commonly known as 'piano stool' complexes. They have a general formula with a core of [(η^6−arene)Ru] with either a bidentate ligand system accompanied by mono dentate ligands, solvents, or a tridentate ligand to satisfy

* Corresponding authors.
E-mail address: smaji@chy.iith.ac.in (S. Maji).

https://doi.org/10.1016/j.jorganchem.2021.122074
0022-328X/

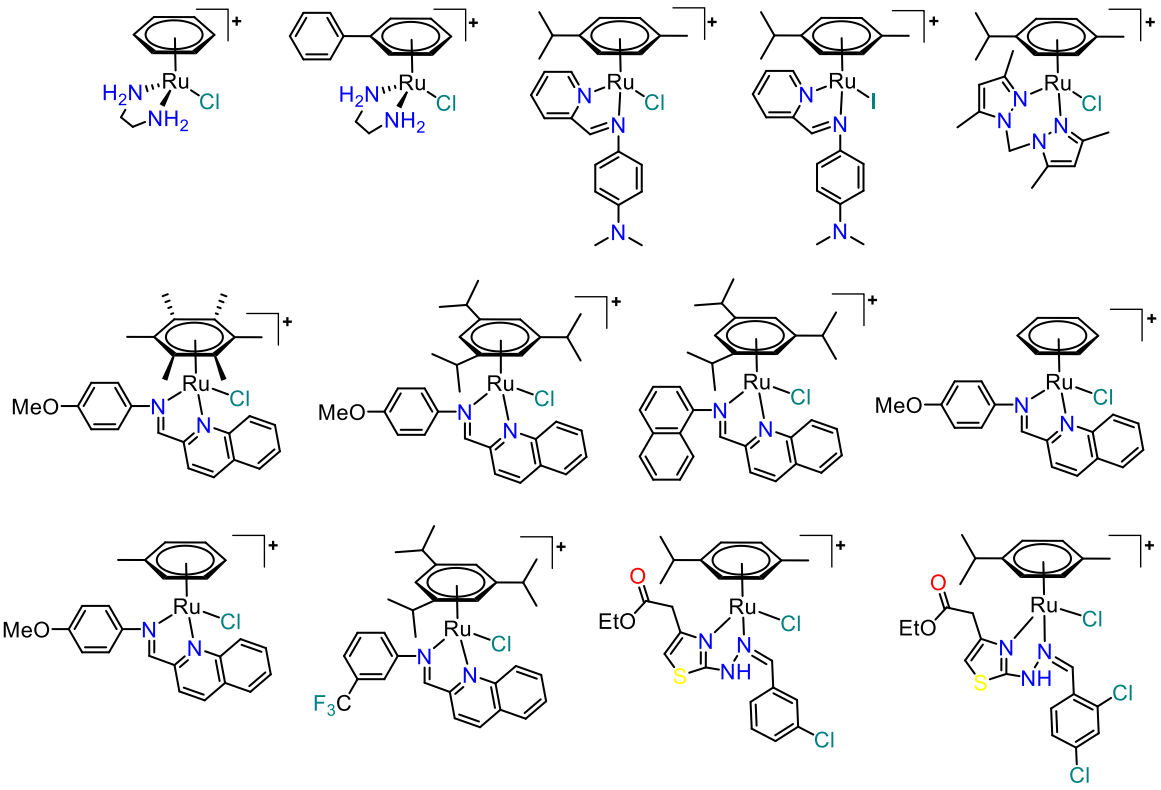

Fig. 1. Selected Arene compounds with N,N−chelating ligands reported in the literature.

the coordination environment of central ruthenium [18]. The balance between hydrophobic (arene part) and hydrophilic (anionic part) nature finely tunes their activity for *in vitro* studies. [19]. Common bidentate ligands used in the systems are N,N−chelating (aliphatic and aromatic diamines, pyridine derivatives) [16,20–22]. However, there are multiple examples of N,O− (amino acid ligands, amine alcohols, pyridine derivatives of aldehydes, acids, etc.), [15] O,O− (mainly β-diketones), [19] and C, N− (benzimidazole based) chelating ligands, [23,24] and they also showed promising antitumor and DNA cleavage activity. The attachment of the 1,3,5-triaza-7-phosphaadamantane (PTA) ligand to central ruthenium as a mono dentate ligand, well-known as RAPTA (ruthenium arene PTA) complexes, [11] has opened a new spectrum for cancer treatment. The hydrophilicity of these classes of compounds and protonation in lower pH allows them *in vitro* hydrolysis and efficient generation of the active intermediates [25,26]. Several modes of action for cell death are found in the derivatives of RAPTA complexes [27–29]. Multinuclear arene complexes were also investigated, [30–32] and their unique self-assembly properties generated two- and three-dimensional structures with good solubility and the large cavity helps to encapsulate small molecules [33,34]. Recently, the ruthenium arene complexes have been exploited as powerful catalysts for water oxidation, proton reduction and carbon dioxide reduction, which is frequently proposed as a promising option for harvesting solar energy aiming to mimic the critical aspects of the natural processes. Some selected mononuclear arene complexes with N,N− chelating ligands employed earlier for anticancer drug has been summarized in Fig 1.

Herein we report the synthesis and characterization of two appropriately designed bis bidentate ligands **L¹** (2-(3,5-di(pyridin-2-yl)-4H-1,2,4-triazol-4-yl)isoindoline-1,3-dione) and **L²** (2,2′-(4-(1H-pyrrol-1-yl)-4H-1,2,4-triazole-3,5-diyl)dipyridine) and their corresponding mononuclear ruthenium chloro arene complexes [Ru(η^6-*p*-cymene)(**L¹**)Cl]Cl: [**1**]Cl, [Ru(η^6-*p*-cymene)(**L²**)Cl]Cl: [**2**]Cl and [Ru(η^6-*p*-cymene)(**L²**)Cl](PF_6): [**2**](PF_6) towards potent application of anticancer drug (Fig. 2). Extended conjugation and protected ring have been introduced to the structural unit to increase hydrophobicity and improve transport to the cells. Thorough characterization of the new ligand **L¹**, complex [**1**]Cl and [**2**]Cl have been achieved *via* ^{1}H NMR, ^{13}C NMR, two-dimensional NMR spectral studies (HSQC, COSY and HMBC). Furthermore, we have exchanged the counterion for varying the solubilities in the aqueous medium. Detailed spectroscopic and redox properties have been investigated for all the prepared metal complexes along with the ligands. The single-crystal X-ray structures have elucidated the molecular structures of [**2**]Cl and [**2**](PF_6). Finally, we performed detailed analysis of the potency of these ruthenium complexes in A549 lung adenocarcinoma and MDA-MB-231 breast adenocarcinoma cells. Our results revealed that these complexes exhibit substantial cytotoxicity in cancer cells and could potentially be used for development of drugs against cancer.

2. Experimental

2.1. Materials

$RuCl_3.3H_2O$, 2-cyanopyridine, hydrazine hydrate and α-terpinene were purchased from Sigma-Aldrich (Merck). Phthalic anhydride, 2, 5-dimethoxytetrahydrofuran and sodium hydride were purchased from SRL chemicals. Dry acetonitrile was obtained by distillation over CaH_2, whereas methanol and ethanol were dried by using sodium following standard laboratory protocol. All the chemicals and reagents were used as received without further purification unless otherwise mentioned. The precursor dichloro(*p*-cymene)ruthenium(II) dimer [35] and **L²** [36] were synthesized following the previously reported literature procedure with slight modifications. Human lung adenocarcinoma cells; A549 and breast adenocarcinoma cells; MDA-MB-231 were procured from Amer-

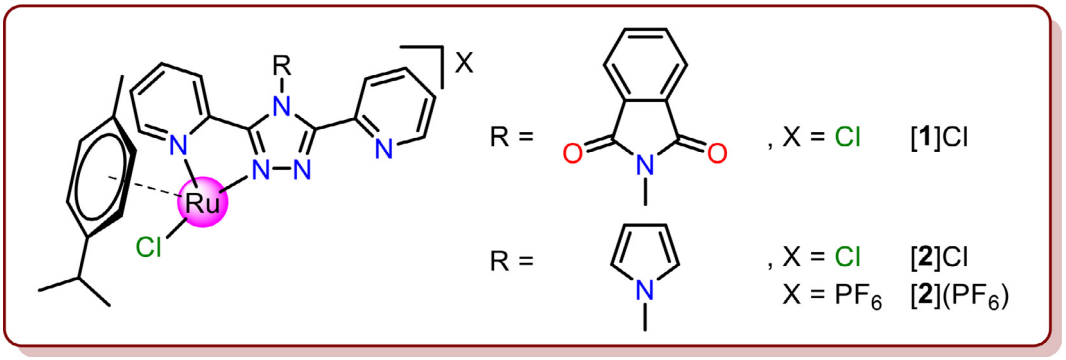

Fig. 2. Complexes used in this study

ican Type Culture Collection (ATCC®). DMEM, RPMI-1640 and Penicillin-Streptomycin solution were obtained from Lonza. Fetal Bovine Serum was purchased from Himedia. Tissue culture plates and reagents including MTT reagent, hydrochloric acid, isopropanol and methanol were procured from Thermo Fisher Scientific. DMSO, crystal violet stain and NP-40 were obtained from Sigma-Aldrich (Merck).

2.2. Physical measurements

BRUKER AVANCE III-400 MHz spectrometer was used to record ^{1}H, ^{13}C NMR, two-dimensional NMR spectra at 295 K in $CDCl_3$; chemical shift values (δ, ppm) and coupling constants (Hz) are reported in the standard fashion with reference to either tetramethylsilane (TMS) (δ(H) 0.00 ppm) or $CHCl_3$ (δ(H) 7.26 ppm). In ^{1}H NMR, the following abbreviations are used throughout: s = singlet, d = doublet, t = triplet, m = multiplet and dd = doublet of doublet, td = triplet of doublet. High-resolution mass spectra (HR-MS) were recorded in Q-TOF electron spray ionization (ESI) and atmospheric pressure chemical ionization (APCI) modes (Model: HRMS Q-TOF 6538). FT-IR measurement (KBr) was carried out on a Jasco spectrometer (Model: FTIR 4600 ST LE). The UV-vis spectra were collected using a Jasco V-730 UV-vis spectrophotometer. All cyclic voltammetry (CV) experiments were performed on CHI-660 electrochemical analyzer under nitrogen atmosphere at scan rate of 100 mV s^{-1} at room temperature in acetonitrile using tetra butyl ammonium perchlorate (TBAP) as supporting electrolyte in three-electrode one-component system. A glassy carbon electrode (3 mm diameter) was used as working electrode, platinum wire as auxiliary electrode and saturated calomel electrode (SCE) as a reference electrode. The elemental analysis was performed on a BRUKER EURO EA machine. Thermo Fisher Scientific Steri Cycle CO_2 incubator was used to culture the cells. Live-cell imaging was carried out using Nikon ECLIPSE TS2R-FL Inverted Research Microscope.

2.3. Preparation of the ligands

2-Cyanopyridine (5 mL, 52 mmol) and hydrazine hydrate (8 mL of 50–60 %) were taken in a round-bottomed flask in 10 mL of absolute ethanol. Sulfur powder (200 mg) was added to the solution and kept under reflux for 3 h. Initially, the solution turned brown and orange crystals start precipitating after 2 h. The crystalline product was filtered, which was air-dried and used without further purification. After that, the orange product was boiled with 2 M HCl solution for 1 h and the initially formed brown solution became colorless. The solution was then cooled and basified with ammonium hydroxide solution and a white curd-like precipitate of 3,5-Di(2-pyridyl)-4-amino-1,2,4-triazole (**L**) was formed. The precipitate was recrystallized from dichloromethane in good yield and used for the next step. Both the ligands $\mathbf{L^1}$ (2-(3,5-di(pyridin-2-yl)-4H-1,2,4-triazol-4-yl)isoindoline-1,3-dione) and $\mathbf{L^2}$ (2,2′-(4-(1H-pyrrol-1-yl)-4H-1,2,4-triazole-3,5-diyl)dipyridine) have been prepared from this common synthon.

2.3.1. Preparation of $\boldsymbol{L^1}$

3,5-Di(2-pyridyl)-4-amino-1,2,4-triazole (500 mg, 2.1 mmol) was taken in a round-bottom flask and dissolved in 3 mL acetic acid. Then phthalic anhydride (311 mg, 2.1 mmol) was added, and the solution was refluxed overnight to obtain white precipitate $\mathbf{L^1}$ which was further crystallized from dichloromethane. Yield: 590 mg (76%). ^{1}H NMR (400 MHz, $CDCl_3$): δ (ppm) = 8.39 (2H, d, J = 7.9 Hz, H1 and H1′), 8.25 (2H, d, J = 4.8 Hz, H4 and H4′), 8.00 (2H, dd, J = 5.5, 3.0 Hz, H3 and H3′), 7.85–7.92 (2H, m, H6 and H6′), 7.80 (2H, td, J = 7.8, 1.8 Hz, H5 and H5′), 7.24 (2H, ddd, J = 7.6, 4.9, 1.2 Hz, H2 and H2′). ^{13}C NMR of $\mathbf{L^1}$, (101 MHz, $CDCl_3$): δ (ppm) = 163.55, 151.59, 149.37, 145.81, 136.94, 134.78, 130.49, 124.79, 124.38, 123.54. Mp: 239–242 °C. FT-IR (KBr, cm^{-1}): 1750 (s) ν(C=O), 1698 (s) ν(C=C), 1470 (m) ν(C=N) (m, medium; s, strong). UV-vis (MeOH) λ (nm) [ε (M^{-1} cm^{-1})]: 240 [27496], 290 [35850].

2.3.2. Preparation of $\boldsymbol{L^2}$

3, 5-di (pyridin-2-yl)-4H-1, 2, 4-triazol-4-amine (500 mg, 2.1 mmol) was taken in a round-bottom flask and dissolved in 1, 4-dioxane-acetic acid (1:1) mixture. Next, 2, 5-dimethoxytetrahydrofuran (330 mg, 2.5 mmol) was added and the solution was refluxed for 24 h. After work up the final product $\mathbf{L^2}$ was purified by column chromatography over neutral alumina by 1% ethanol-chloroform eluent. Yield: 484 mg (84%). ^{1}H NMR (400 MHz, $CDCl_3$): δ (ppm) = 8.42 (2H, d, J = 2.4 Hz, H1 and H1′), 7.73 (2H, d, J = 3.9 Hz, H4 and H4′), 7.65 (2H, dt, J = 7.8, 1.0 Hz, H3 and H3′), 7.20 (2H, dt, J = 4.1, 2.5 Hz, H2 and H2′), 6.78 (2H, t, J = 1.1 Hz, H5 and H5′), 6.13 (2H, t, J = 1.1 Hz, H6 and H6′). FT-IR (KBr, cm^{-1}): 1587 (s) ν(C=C), 1466 (m) ν(C=N) (m, medium; s, strong). UV-vis (MeOH) λ (nm) [ε (M^{-1} cm^{-1})]: 247 [39882], 279 [49890].

2.4. Synthesis of complexes

2.4.1. Preparation of Ruthenium(II) complex [1]Cl

In argon atmosphere, $\mathbf{L^1}$ (37 mg, 0.1 mmol) was dissolved in 15 mL dry methanol in a 50 mL round-bottom flask. Dichloro(*p*-cymene)ruthenium(II) dimer (70 mg, 0.11 mmol) was added and stirred in room temperature for 8 h. The brown solution obtained were dried in vacuo and purified by column chromatography over neutral alumina column using 3% ethanol/dichloromethane as eluent. Yield: 58 mg (67%). *Anal. Calc.* (%) for $C_{30}H_{26}Cl_2N_6O_2Ru$ C, 53.42; H, 3.89; N, 12.46; Found (%): C, 52.99; H, 4.08; N, 12.24; ^{1}H NMR (400 MHz, $CDCl_3$): δ (ppm) = 9.14 (1H, d, J = 6.3 Hz, H8),

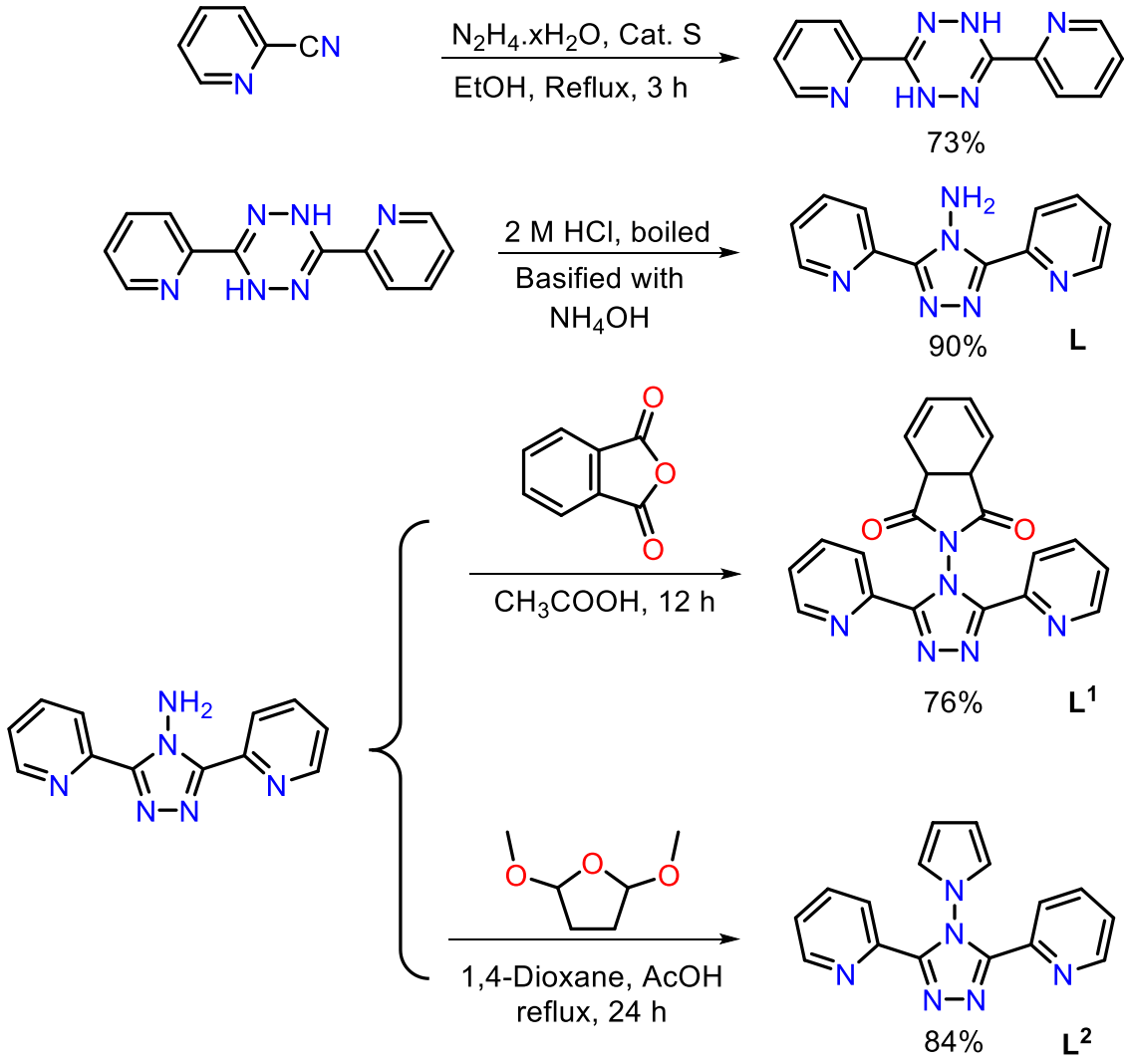

Scheme 1. Synthesis of **L**, **L¹** and **L²**.

8.8 (1H, d, J = 5.3 Hz, H19), 8.63 (1H, d, J = 9.6 Hz, H11), 8.45 (1H, d, J = 9.5 Hz, H16), 8.02 (1H, d, J = 8.7 Hz, H13), 7.95 (1H, t, J = 7.6 Hz, H14), 7.79 (1H, t, J = 8.3 Hz, H10), 7.34–7.55 (5H, m, H9, H12, H15, H17 and H18), 5.91 (1H, d, J = 4.7 Hz, H4), 5.76 (1H, d, J = 7.7 Hz, H7), 5.69 (1H, d, J = 2.9 Hz, H6), 5.59 (1H, d, J = 6.5 Hz, H5), 2.87 (1H, dd, J = 3.4 Hz, *p*-cym H2), 2.27 (3H, s, *p*-cym H3), 1.17–1.22 (6H, m, *p*-cym H1). ^{13}C NMR of [**1**]Cl, (101 MHz, $CDCl_3$): δ (ppm) = 172.16, 170.15, 154.80, 154.54, 150.63, 149.94, 145.68, 145.25, 139.58, 137.55, 136.80, 132.76, 130.40, 129.11, 128.08, 126.46, 124.83, 124.35, 123.99, 115.99, 104.74, 101.35, 86.01, 84.61, 84.08, 82.76, 30.95, 22.33, 22.01, 18.61. ESI–MS(+) mass spectrum in MeOH: ([M + MeOH]$^+$), *m/z*: 671.11 (calc. 671.11). FT-IR (KBr, cm^{-1}): 1721 (s) ν(C=O), 1614 (m) ν(C=C), 1450 (m) ν(C=N) (m, medium; s, strong). UV-vis (MeOH) λ (nm) [ε (M^{-1} cm^{-1})]: 292 [36064], 343 [10257].

*2.4.2. Preparation of Ru(II) complexes [**2**]Cl and [**2**](PF$_6$)*

[**2**]Cl: In argon atmosphere, **L²** (33 mg, 0.1 mmol) was dissolved in 15 mL dry methanol in a 50 mL round-bottom flask. Dichloro(*p*-cymene)ruthenium(II) dimer (70 mg, 0.11 mmol) was added and stirred in room temperature for 8 h. The brown solution obtained were dried in vacuo and purified by column chromatography over neutral alumina column using 5% ethanol/dichloromethane eluent. Yield: 60 mg (71%) [**2**]Cl. *Anal. Calc.* (%) for $C_{26}H_{26}Cl_2N_6Ru$ C, 52.53; H, 4.41; N, 14.14; Found (%): C, 52.48; H, 4.79; N, 13.94; ^{1}H NMR of [**2**]Cl, (400 MHz, $CDCl_3$): δ (ppm) = 9.71 (1H, d, J = 2.9 Hz, H8), 8.52 (1H, d, J = 6.2 Hz, H19), 8.16 (1H, d, J = 5.2 Hz, H11), 7.85 (2H, dt, J = 9.8 Hz, H16), 7.70 (1H, t, J = 2.9 Hz, H10), 7.64 (1H, d, J = 5.1 Hz, H9 and H17), 7.40 (1H, m, H18), 6.89 (1H, t, J = 6.4 Hz, H12), 6.40 (2H, m, H13 and H15), 6.30 (3H, m, H4, H7 and H14), 6.12 (1H, d, J = 8.1 Hz, H5), 5.94 (1H, d, J = 5.6 Hz, H6), 3.09 (1H, m, *p*-cym H2), 2.33 (3H, s, *p*-cym H3), 1.73 (6H, s, *p*-cym H1). ^{13}C NMR of [**2**]Cl, (101 MHz, $CDCl_3$): δ (ppm) = 157.98, 153.61, 152.86, 150.01, 143.18, 142.21, 139.67, 137.24, 128.79, 126.14, 124.70, 122.53, 122.18, 120.64, 110.55, 110.40, 104.71, 102.01, 87.90, 85.72, 83.90, 83.83, 31.06, 22.94, 21.66, 18.74. ESI–MS(+) mass spectrum in MeOH: [M – Cl]$^+$, *m/z*: 559.10 (calc. 559.10). FT-IR (KBr, cm^{-1}): 1613 (m) ν(C=C), 1450 (m) ν(C=N) (m, medium; s, strong). UV-vis (MeOH) λ (nm) [ε (M^{-1} cm^{-1})]: 294 [26657], 348 [6722].

[**2**](PF$_6$): The precursor [**2**]Cl was dissolved in methanol and saturated methanolic KPF_6 was added and stirred for 2 h. The solution was filtered and kept for crystallization to obtain [**2**](PF$_6$). Yield: 54%. *Anal. Calc.* (%) for $C_{26}H_{26}ClF_6N_6PRu$ C, 44.36; H, 3.72; N, 11.94; Found (%): C, 44.14; H, 3.95; N, 11.42; ESI–MS(+) mass spectrum in MeOH: [M – PF$_6$]$^+$, *m/z*: 559.10 (calc. 559.10). FT-IR (KBr, cm^{-1}): 1616 (m) ν(C=C), 1450 (m) ν(C=N), 836 (s) ν(PF$_6$) (m, medium; s, strong). UV-vis (MeOH) λ (nm) [ε (M^{-1} cm^{-1})]: 294 [25861], 348 [5961], 557 [420].

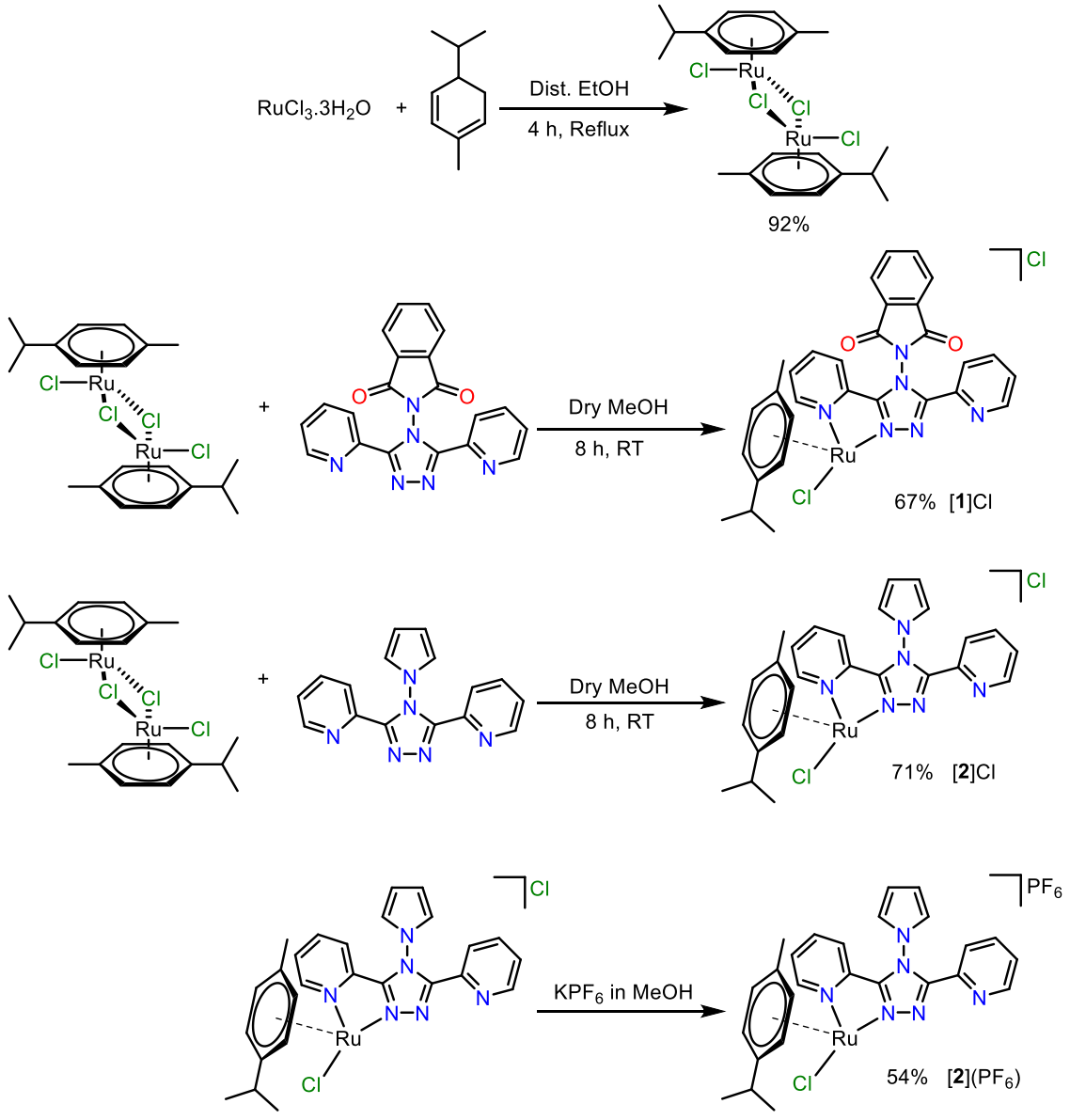

Scheme 2. Synthesis of the [1]Cl, [2]Cl and [2](PF_6).

2.5. Crystallography

Single crystals of both the complexes [**2**]Cl and [**2**](PF_6) were crystallized by the slow evaporation of a 1:2 methanol-dichloromethane solvent mixture. A crystal of suitable dimensions was mounted on a CryoLoop (Hampton Research Corp.) with a layer of light mineral oil. The crystallographic data were measured with an Agilent Supernova dual-source diffractometer. Single crystal X-ray diffraction study was carried out on a Rigaku Supernova Xcalibur Eos CCD detector with graphite-monochromatic CuKα (1.54184 Å) radiation for [**2**]Cl and MoKα (λ = 0.71073 Å) radiation for [**2**](PF_6). The structures were solved by direct methods SHELXT [37] and refined on F^2 using the full-matrix least-squares methods with SHELXL [38]. Absorption corrections were performed based on multi-scans. All hydrogen atoms were placed at idealized positions, while all other atoms were refined anisotropically. The MERCURY program was used to draw the molecules.

2.6. Cell culture

Human lung adenocarcinoma cell line; A549 was cultured in Dulbecco's Modified Eagle Medium (Lonza) and breast adenocarcinoma cell line; MDA-MB-231 was cultured in RPMI-1640 medium (Lonza), both containing 10% Fetal Bovine Serum (Himedia) and 1% antibiotic mixture of Penicillin-Streptomycin (Lonza). These cells were seeded in 12-well and/or 96-well plates (Thermo Fisher Scientific) depending on the experiment to be done and were cultured in humid conditions with constant 5% CO_2 at 37 °C.

2.7. Live-cell imaging

To study the effects of ruthenium(II) arene complexes, cancer cells were seeded in a 12-well plate at a cell density of 10^4 cells/well, in DMEM/RPMI-1640 + 10% FBS + 1% Pen/Strep media in a 5% CO_2 incubator at 37 °C. The complexes were dissolved in dimethyl sulfoxide (DMSO) to carry out the experiments. The cells were treated with [**1**]Cl, [**2**]Cl and [**2**](PF_6) at indicated concentra-

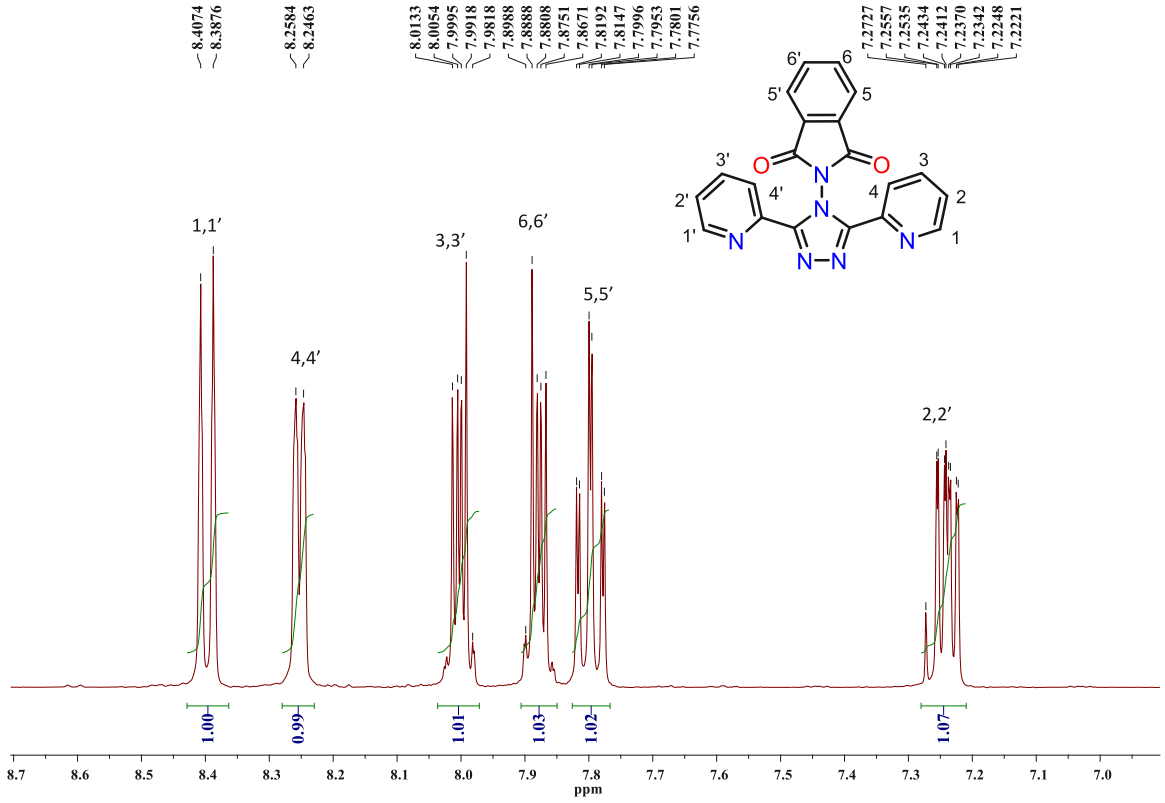

Fig. 3. ^{1}H NMR of ligand **L¹** in $CDCl_3$.

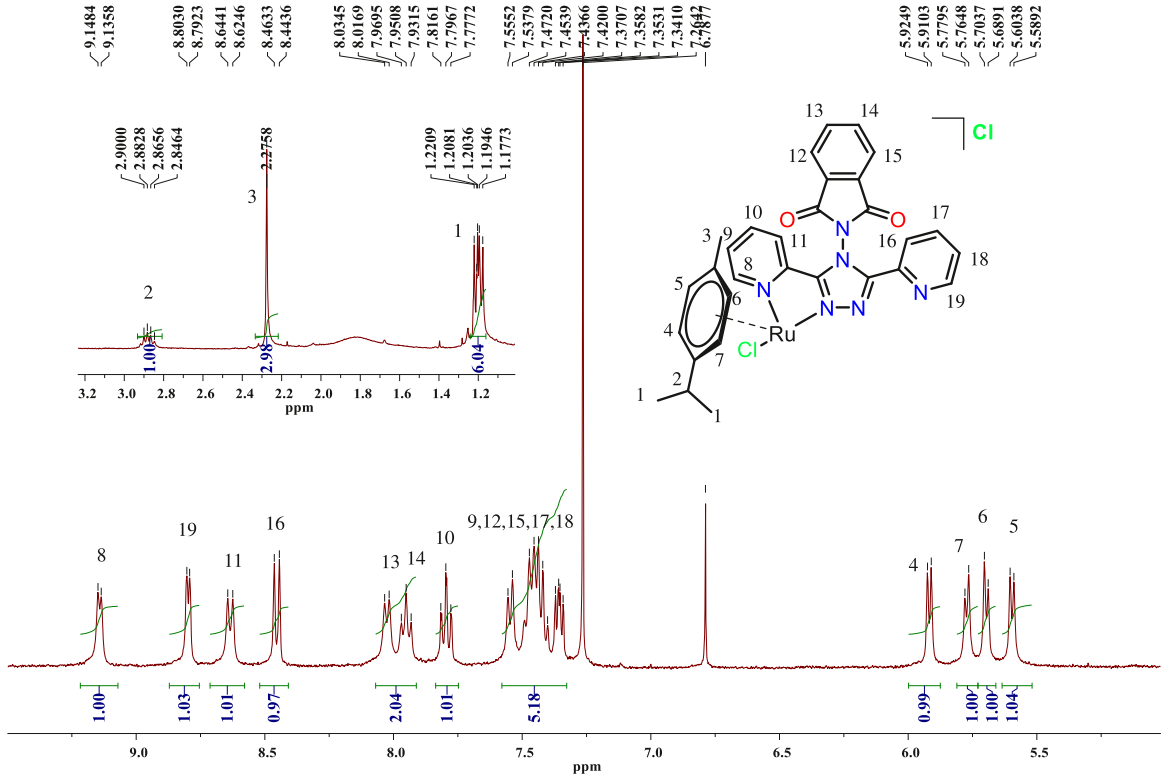

Fig. 4. ^{1}H NMR of [1]Cl in $CDCl_3$.

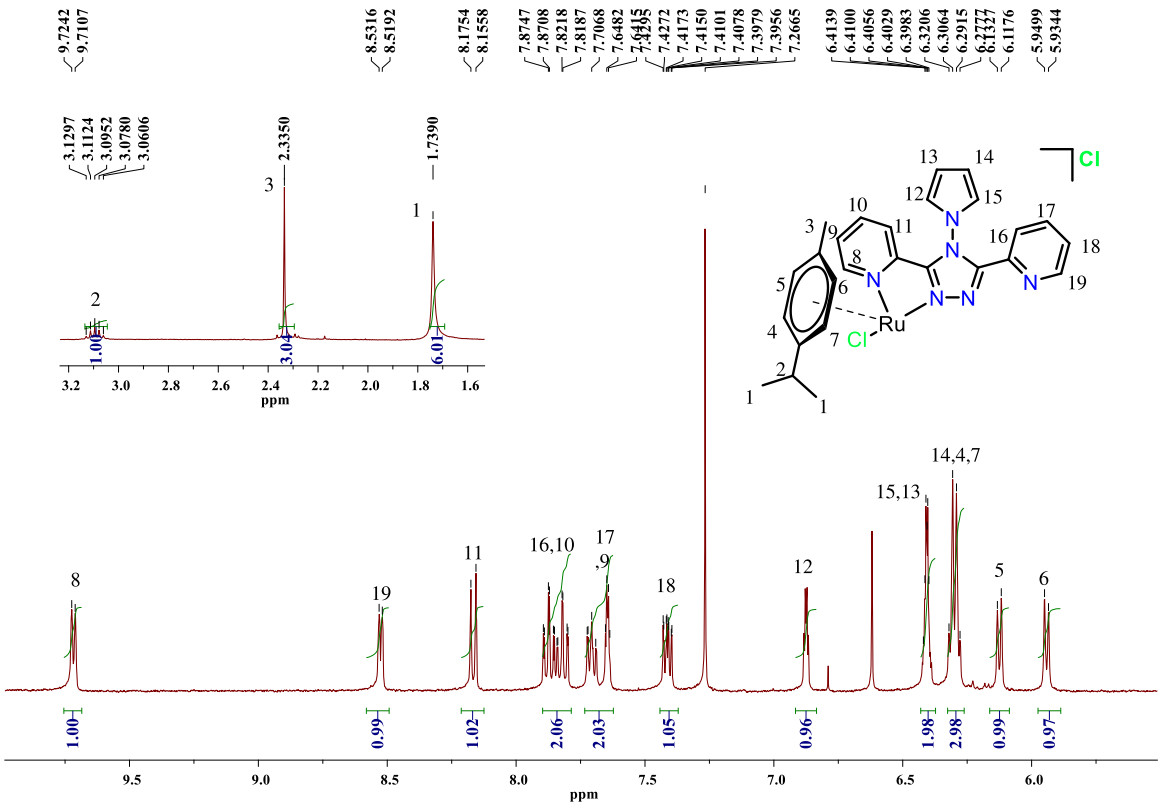

Fig. 5. ^{1}H NMR of [2]Cl in $CDCl_3$.

Table 1
Selected crystallographic data for [2]Cl and [2](PF_6)

Complex	[2]Cl	[2](PF_6)
Empirical formula	$C_{26}H_{26}Cl_2N_6Ru$	$C_{26}H_{26}ClF_6N_6PRu$
Formula weight	594.5	704.02
Temperature/K	273	273
Crystal system	triclinic	monoclinic
Space group	P-1	$P2_1/n$
a/Å	8.6716(3)	16.4053(4)
b/Å	12.4944(6)	10.5310(3)
c/Å	13.9241(7)	16.9552(4)
α/°	113.755(5)	90
β/°	91.254(3)	100.972(2)
γ/°	104.937(3)	90
Volume/Å^3	1320.60(11)	2875.70(13)
Z	2	4
ρ_{calc}g/cm^3	1.495	1.626
μ/mm^{-1}	6.871	0.761
F(000)	604.0	1416.0
Crystal size/mm^3	0.06 × 0.05 × 0.02	0.04 × 0.03 × 0.02
Radiation	CuKα (λ = 1.54184)	MoKα (λ = 0.71073)
2θ range for data collection/°	7.008 to 139.986	4.576 to 58.426
Index ranges	-8 ≤ h ≤ 10, -15 ≤ k ≤ 15, -16 ≤ l ≤ 16	-22 ≤ h ≤ 22, -12 ≤ k ≤ 14, -21 ≤ l ≤ 19
Reflections collected	12158	12492
Independent reflections	4982 [R_{int} = 0.0423, R_{sigma} = 0.0392]	6650 [R_{int} = 0.0257, R_{sigma} = 0.0420]
Data/restraints/parameters	4982/0/319	6650/0/373
Goodness-of-fit on F^2	1.028	1.043
Final R indexes [I>=2σ (I)]	R_1 = 0.0320, wR_2 = 0.0840	R_1 = 0.0389, wR_2 = 0.0908
Final R indexes [all data]	R_1 = 0.0345, wR_2 = 0.0863	R_1 = 0.0541, wR_2 = .1021
Largest diff. peak/hole / e Å^{-3}	0.70/-0.76	0.67/-0.44

tions for 72 h once 70–75% cell density was achieved. Afterwards, the growth medium was removed and cells were washed multiple times with 1X Phosphate Buffered Saline (PBS) to remove residual ruthenium complexes and bright field images were captured using Nikon Inverted Research Microscope at 20 ms exposure. Furthermore, to observe relative cell death, the cells were stained using 0.1% Crystal Violet stain (prepared in 20% Methanol v/v) and the image was captured using Bio-RAD Chemidoc XRS+ imaging system after multiple washes with 1X PBS to remove the residual stain.

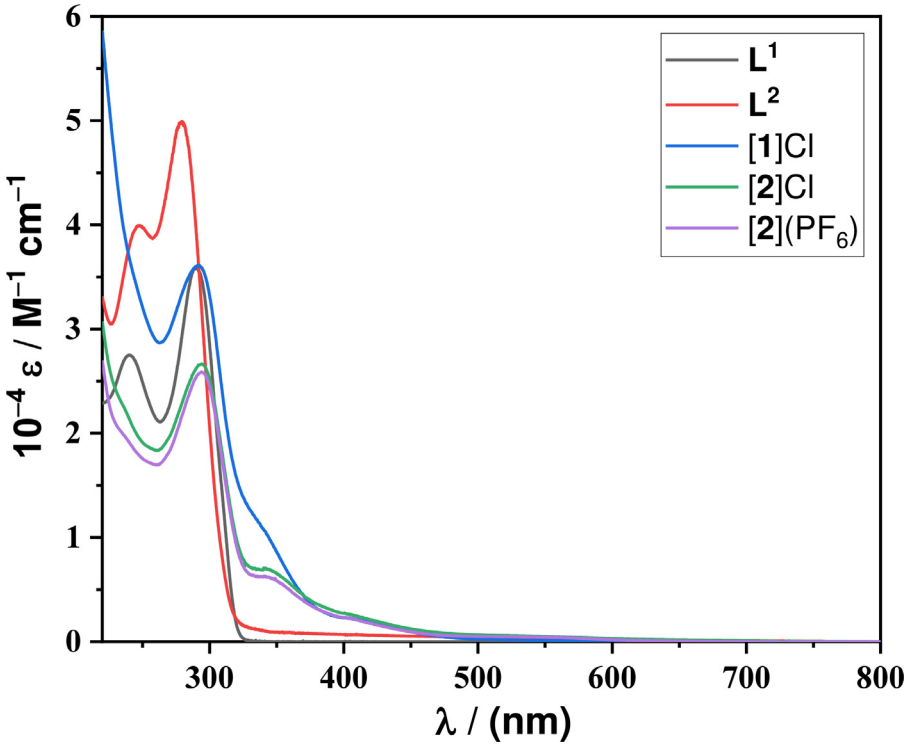

Fig. 6. UV-vis spectra of **L¹**, **L²**, [1]Cl, [2]Cl and [2](PF_6) in methanol solvent at room temperatur-e.

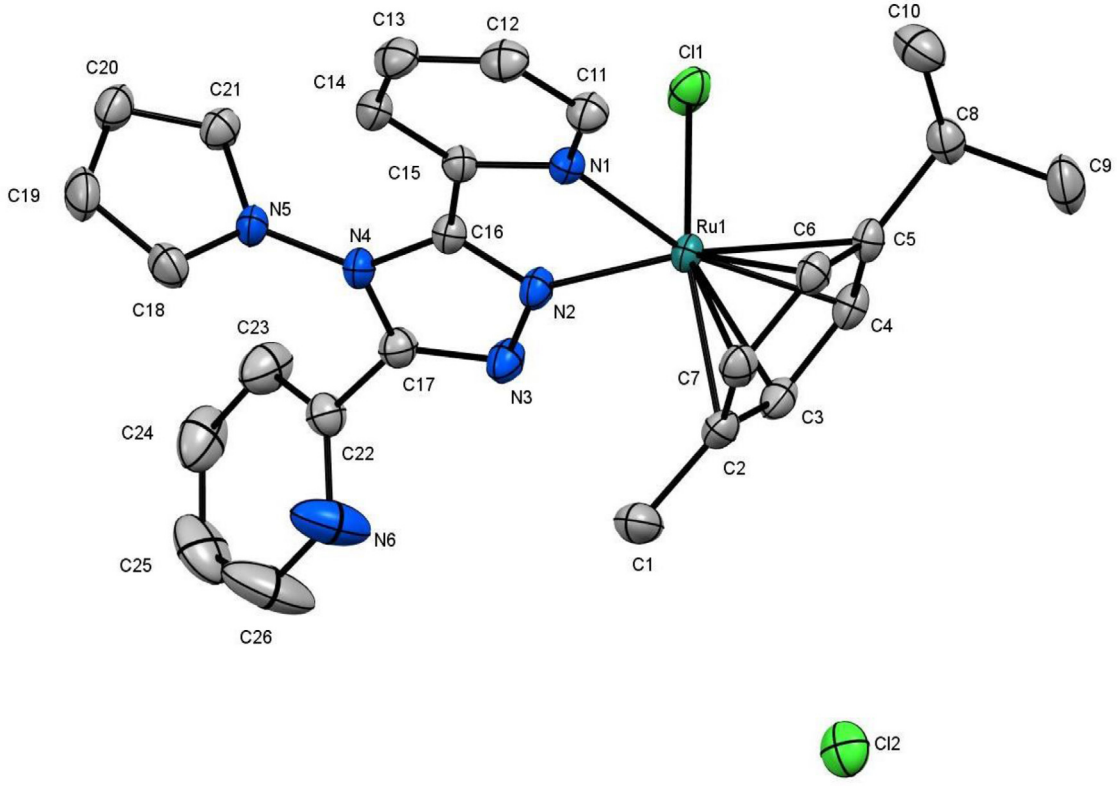

Fig. 7. Single crystal X-ray crystal structures of [2]Cl. The thermal ellipsoids are drawn with 40% probability. Hydrogen atoms are omitted for clarity.

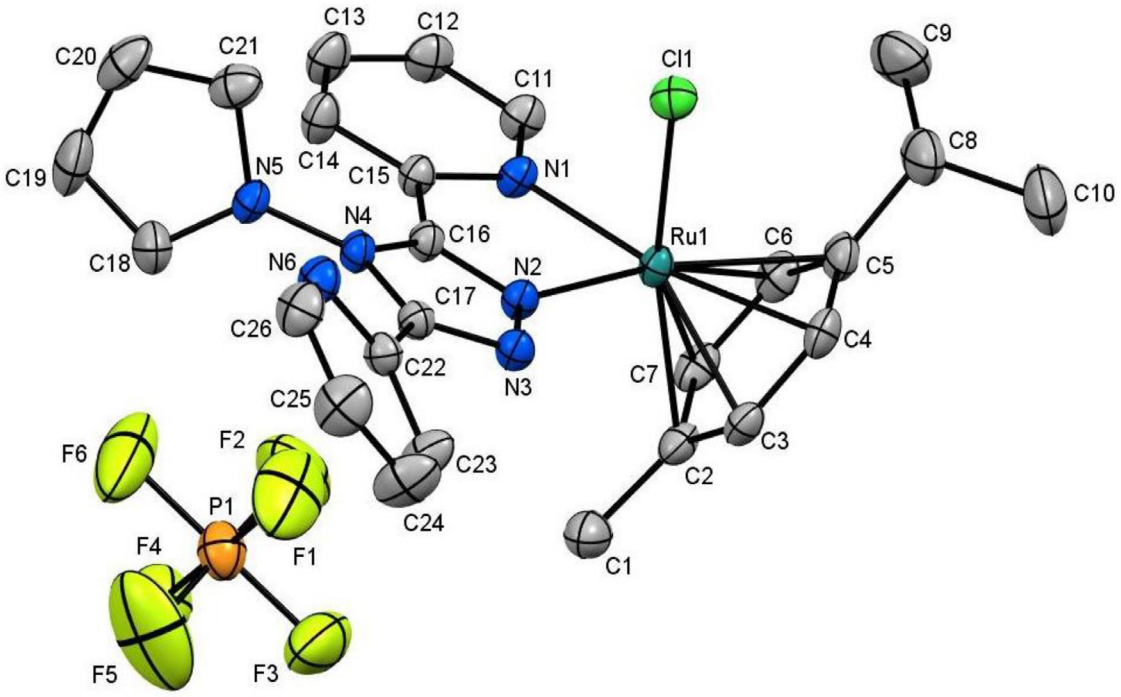

Fig. 8. Single crystal X-ray crystal structures of [2](PF_6). The thermal ellipsoids are drawn with 40% probability. Hydrogen atoms are omitted for clarity.

2.8. Cell cytotoxicity experiment

10^3 cancer cells were seeded in each well of a 96-well plate and cultured for 16 h in media containing DMEM/RPMI-1640 + 10% FBS + 1% Pen/Strep at 37 °C in a 5% CO_2 incubator. To examine the cytotoxic effects, the cells were treated with [**1**]Cl, [**2**]Cl and [**2**](PF_6), for 72 h. Thereafter, the media containing the compounds was removed and the cells were washed using 1X PBS. Subsequently, 100 µL of 0.5 mg/mL MTT reagent (3-(4,5-dimethylthiazol-2-yl)-2,5-diphenyltetrazolium bromide) was added onto the cells and incubated for 4 h. Afterwards, MTT reagent was aspirated and 100 µL MTT solvent (4 mM HCl, 0.1% Nonidet P-40 (NP-40) prepared in isopropanol) was added to each well of the 96-well plate and rotated gently for 20 min on an orbital shaker to dissolve the formed formazan crystals. Absorbance was recorded at 595 nm using iMARK micro plate reader (Bio-Rad). The cellular cytotoxicities of [**1**]Cl, [**2**]Cl and [**2**](PF_6) were calculated as a ratio of recorded absorbance at 595 nm of treated cells to the DMSO control and IC_{50} values and standard deviation were determined using GraphPad Prism.

3. Results and discussion

3.1. Synthesis and characterization

The triazole-based phthalimide protected new ligand $\mathbf{L^1}$ was synthesized by reaction of phthalic anhydride and 3,5-Di(2-pyridyl)-4-amino-1,2,4-triazole, which is a rearrangement product of 3,6-Di(2-pyridyl)-1,2-dihydro-1,2,4,5-tetrazine. Similarly, another triazole-based pyrrole protected ligand $\mathbf{L^2}$ was prepared by the reaction of 3,5-Di(2-pyridyl)-4-amino-1,2,4-triazole with 2, 5-dimethoxytetrahydrofuran following previously reported literature procedure with slight modification (Scheme 1 and 2). All the ruthenium complexes [**1**]Cl, [**2**]Cl and [**2**](PF_6) were synthesized following conventional method, by reacting the corresponding ligands with the standard starting material dichloro(*p*-cymene)ruthenium(II) dimer in methanol at room temperature with moderately high yield. For complex [**2**](PF_6), anion exchange was performed with methanolic KPF_6 solution. The formation of all these complexes has been authenticated by their satisfactory ^{1}H and ^{13}C NMR spectra, mass spectra, FT-IR spectra and UV-vis spectral studies. Moreover, for [**2**]Cl and [**2**](PF_6), suitable single-crystal structures have been grown by the slow evaporation from methanol-dichloromethane mixture and have been structurally elucidated by single-crystal X-ray diffraction studies.

3.2. Spectral Aspects

NMR Spectroscopy: ^{1}H NMR spectra in $CDCl_3$ exhibit total twelve aromatic protons with six distinguishable resonances for both the ligands $\mathbf{L^1}$ and $\mathbf{L^2}$ in the range of 6.12 to 8.43 ppm. For $\mathbf{L^1}$, the characteristic doublets of pyridyl −CH groups appear at 8.25 and 8.39 ppm and the multi-plates at 7.25 and 8.01 ppm corresponds to the other two pyridyl −CH from the pyridine moiety. Benzene protons of the extended phthalic moiety match well with doublets of triplets at 7.81 and 7.88 ppm (Fig. 3). In the ^{13}C NMR spectrum in $CDCl_3$, phthalimide −C=O resonance appears at 163 ppm (Fig. S1). All the protons have been successfully identified with the help of two-dimensional NMR spectral studies (HSQC, COSY and HMBC) (Fig S2, S3 and S4). For $\mathbf{L^2}$, the peaks are deshielded compared to $\mathbf{L^1}$ due to the presence of pyrrole moiety. Pyridyl −CH protons are in the range of 7.20 to 8.45 ppm, whereas the two protons of the extended pyrrole moiety appear as triplets at 6.13 and 6.78 ppm (Fig. S5). The unsymmetrical nature of [**1**]Cl and [**2**]Cl gives rise to total twenty-six protons; out of which sixteen aromatic protons appear in the range of 5.58 to 9.72 ppm and the rest ten aliphatic protons appear in the range of 1.17 to 3.12 ppm, revealing the diamagnetic nature of Ru(II) with low-spin d^6 configuration for both the metal complexes. Ten aliphatic protons of *p*-cymene groups are in the range of 1.20 to 3.09 ppm. The typical four aromatic pro-

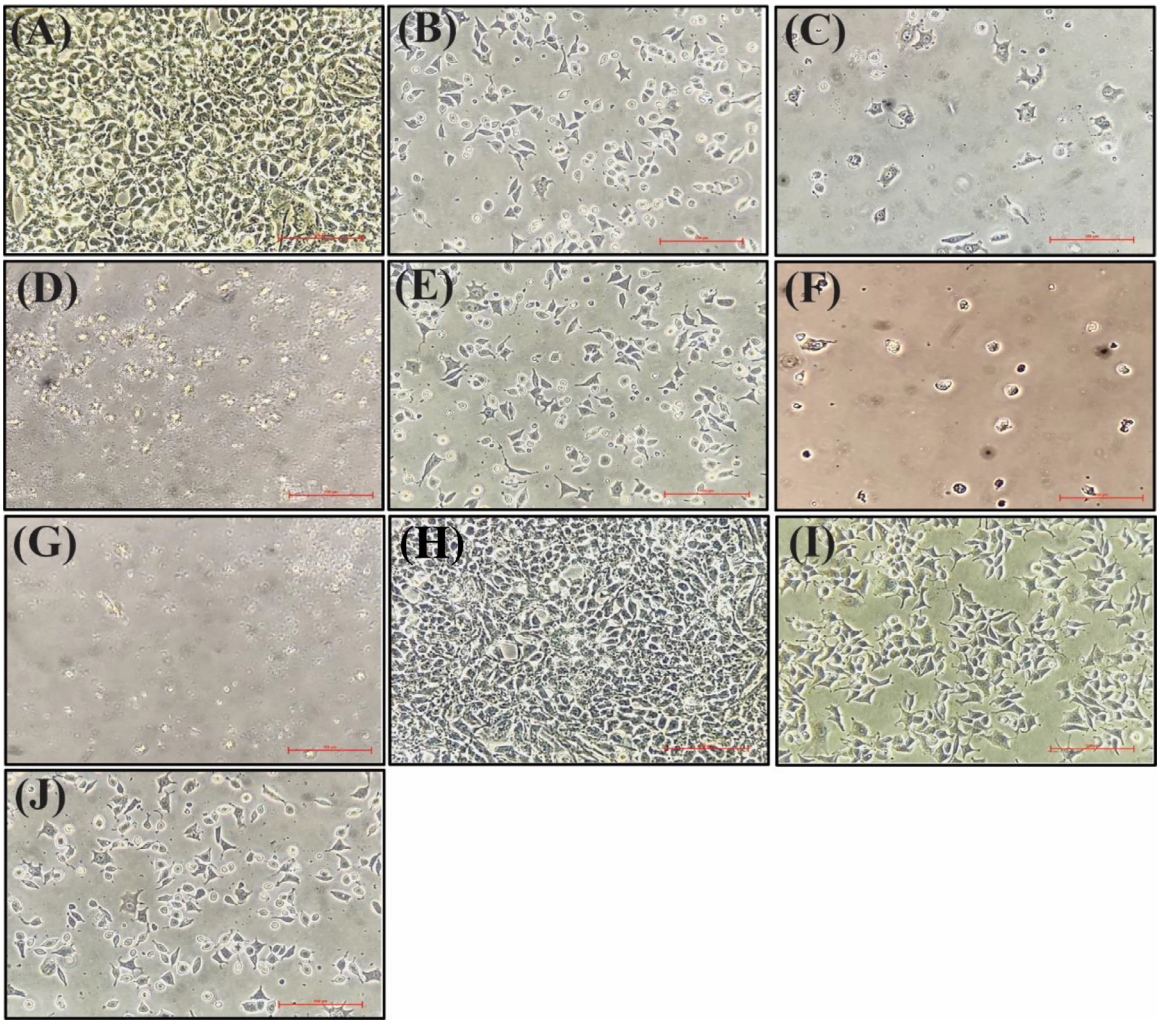

Fig. 9. Bright-field images of A549 adenocarcinoma cells treated with various ruthenium complexes for 72 h. (A) DMSO-treated A549 cells. (B) 5 μM [1]Cl treated A549 cells. (C) 10 μM [1]Cl treated A549 cells. (D) 20 μM [1]Cl treated A549 cells. (E) 5 μM [2]Cl treated A549 cells. (F) 10 μM [2]Cl treated A549 cells. (G) 20 μM [2]Cl treated A549 cells. (H) 5 μM [2](PF_6) treated A549 cells. (I) 10 μM [2](PF_6) treated A549 cells. (J) 20 μM [2](PF_6) treated A549 cells.

tons of arene moiety are within the range of 5.58 to 6.41 ppm for both the complexes, which are in good agreement with the previously reported analogous ruthenium(II) *p*-cymene complexes [39,40]. The distinct isopropyl −CH proton for [**1**]Cl and [**2**]Cl appears at 2.86 and 3.09 ppm, respectively (Figs. 4 and 5). In the ^{13}C NMR spectrum of both [**1**]Cl and [**2**]Cl, the complexes showed 30 and 26 peaks respectively due to the unsymmetrical nature (Figs. S6 and S8). The two distinct phthalimide −C=O resonance of [**1**]Cl appears at 172 ppm and 170 ppm. Additionally, both the complexes are identified by two-dimensional NMR spectral studies (Figs. S7 and S9).

Vibrational spectroscopy: In the solid-state FT-IR spectra of $\mathbf{L^1}$, an intense sharp band was observed at 1750 cm^{-1} that corresponds to the C=O stretching vibration of the phthalic moiety attached to the triazole ring. The C=O band shifted to high energy 1721 cm^{-1} in [**1**]Cl, suggesting the successful incorporation of Ru(II). The characteristic sharp peak at 836 cm^{-1} indicates the presence of PF_6^- in [**2**](PF_6) *via* the counterion exchange from [**2**]Cl (Fig. S10).

UV-vis spectroscopy: UV-vis spectroscopy of all the compounds were recorded in methanol at room temperature. For $\mathbf{L^1}$ and $\mathbf{L^2}$, the π to π^* transitions were observed at 292 and 280 nm, respectively [41]. The complexes [**1**]Cl, [**2**]Cl and [**2**](PF_6) exhibit electronic transition near 350 nm, which could be attributed to Ru(II) based metal to ligand charge transfer (MLCT) transition to the π^* orbital of the respective ligand and intense ligand-based multiple transitions in the high energy UV region [13,42,43]. The band energy (MLCT) decreasing in the order [**2**]Cl ≈ [**2**](PF_6) < [**1**]Cl due to the relative stabilization of dπ {Ru(II)} energy level (Fig. 6).

Mass spectroscopy: The electrospray mass spectra of complexes [**1**]Cl, [**2**]Cl and [**2**](PF_6) were recorded in methanol solvent and [**1**]Cl showed molecular ion peak associated with methanol solvent centered at *m*/*z* 671.11, calculated: 671.11. Both the complexes [**2**]Cl and [**2**](PF_6) showed their molecular ion peaks at 559.10; calculated: 559.10. Thus, satisfying their molecular integrity. No additional significant peaks are observed beyond the molecular peaks which confirm the formation of monomer complexes. Moreover, the relative isotopic abundances match well with the simulated mass spectra (Fig. S11).

3.3. Redox properties

The redox properties of all the complexes and ligands have been investigated in degassed acetonitrile solution at room temperature. Both the ligands are redox-active and the irreversible oxidations are observed at 1.20 V and 1.25 V for $\mathbf{L^1}$ and $\mathbf{L^2}$, re-

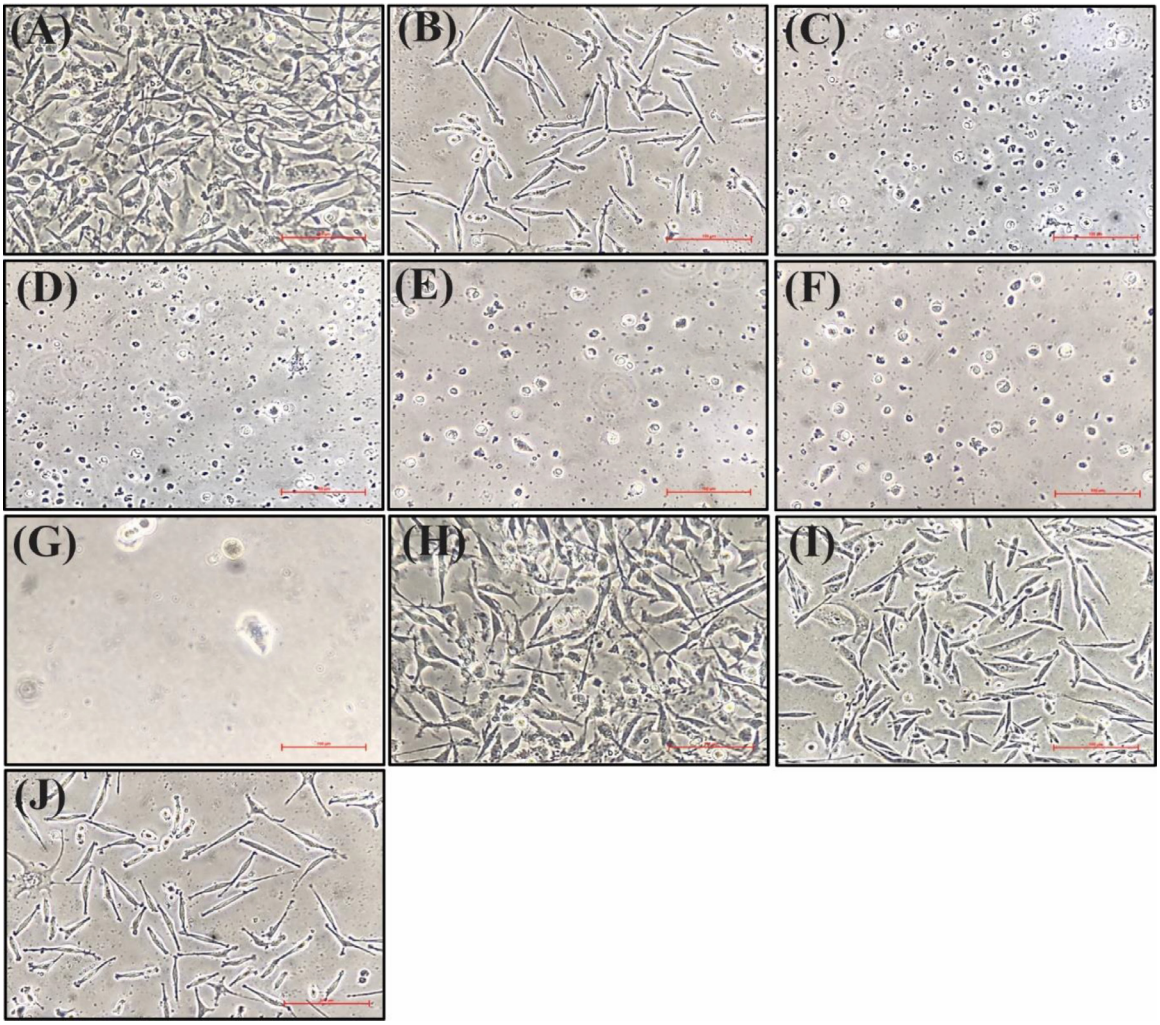

Fig. 10. Bright-field images of MDA-MB-231 adenocarcinoma cells treated with various ruthenium complexes for 72 h. (A) DMSO-treated MDA-MB-231 cells. (B) 2.5 μM [1]Cl treated MDA-MB-231 cells. (C) 5 μM [1]Cl treated MDA-MB-231 cells. (D) 10 μM [1]Cl treated MDA-MB-231 cells. (E) 2.5 μM [2]Cl treated MDA-MB-231 cells. (F) 5 μM [2]Cl treated MDA-MB-231 cells. (G) 10 μM [2]Cl treated MDA-MB-231 cells. (H) 2.5 μM [2](PF_6) treated MDA-MB-231 cells. (I) 5 μM [2](PF_6) treated MDA-MB-231 cells. (J) 10 μM [2](PF_6) treated MDA-MB-231 cells.

spectively [44,45]. Due to the different electronic nature of the mononuclear Ru(II) complexes, the Ru(II)/(III) couples in acetonitrile E^o_{298K}/V are observed at 1.58 V, 1.65 V and 1.63 V respectively for [**1**]Cl, [**2**]Cl and [**2**](PF_6) while the ligand-based oxidations are observed at 1.14 V, 1.17 V and 1.32 V (Fig. S12) [13,42,43]. The more positive potential value in [**2**]Cl/[**2**](PF_6) compared to [**1**]Cl implies the additional stability of the Ru(II) state because of the electronic nature of the pyrrole-based ligand **L²**.

3.4. Crystal structures

The molecular structures of [**2**]Cl and [**2**](PF_6) were elucidated by single-crystal X-ray diffraction and the selected crystallographic data and important bond distances (Å) and bond angles (°) are given in Tables 1 and 2, respectively. Both the complexes display the usual piano stool geometry coordinated *via* arene ring carbons in η^6- fashion, two nitrogen atoms of the chelating ligand and the other position is occupied by chlorine. And the charge has been balanced by either Cl^- or PF_6^-ions. The complex [**2**]Cl crystalized in triclinic system with P-1 space group and the complex [**2**](PF_6) crystallized in monoclinic system with $P2_1/n$ space group. ORTEP representations have been shown in Figs. 7 and 8. The Ru−Cl bond in the case of [**2**]Cl (2.4011 Å) is slightly longer than [**2**](PF_6) (2.3968 Å). The pyridyl Ru−N1 bond is longer than the triazole Ru−N2 bond, as expected from the structural overview. This is due to an unoccupied pyridine ring on the other side of the triazole bridge. Steric factors working on the *p*-cymene moiety resulted in longer Ru−C distances to the three bonds closer to the isopropyl group (Ru−C4, Ru−C5, Ru−C6) than the carbon centers in proximity to the methyl group. (Ru−C2, Ru−C3, Ru−C7). The crystal structures show a planar rotation of the triazole ligand system to the rest of the molecule in the case of [**2**]Cl to [**2**](PF_6). All the bond angles and bond distances are in very good agreement with the previously reported related ruthenium(II) *p*-cymene complexes [46,47].

The complex [**2**]Cl shows intra-molecular hydrogen bonding in C−H hydrogen (C1−H1C • • • N3) (distance 2.654 Å). These molecules are connected *via* intermolecular weak C13−H13 • • • Cl1 hydrogen bonds (distance 2.672 Å, angle 154.44°). The displaced stacking $\pi-\pi$ interactions are also found within the crystal symmetry between the coordinated pyridine groups of neighboring metal centers (distance 3.830 Å). In the complex [**2**](PF_6), the PF_6^- involves hydrogen bonding with C−H hydrogen (C18−H18 • • • F6) (distance 2.391 Å). Intermolecular weak hydrogen bonds in C13−H13 • • • Cl1 (distance 2.692 Å, angle 135.48°) is also present in the structure like its precursor with increased distance and closer angle. In this case, the displaced stacking $\pi-\pi$ interac-

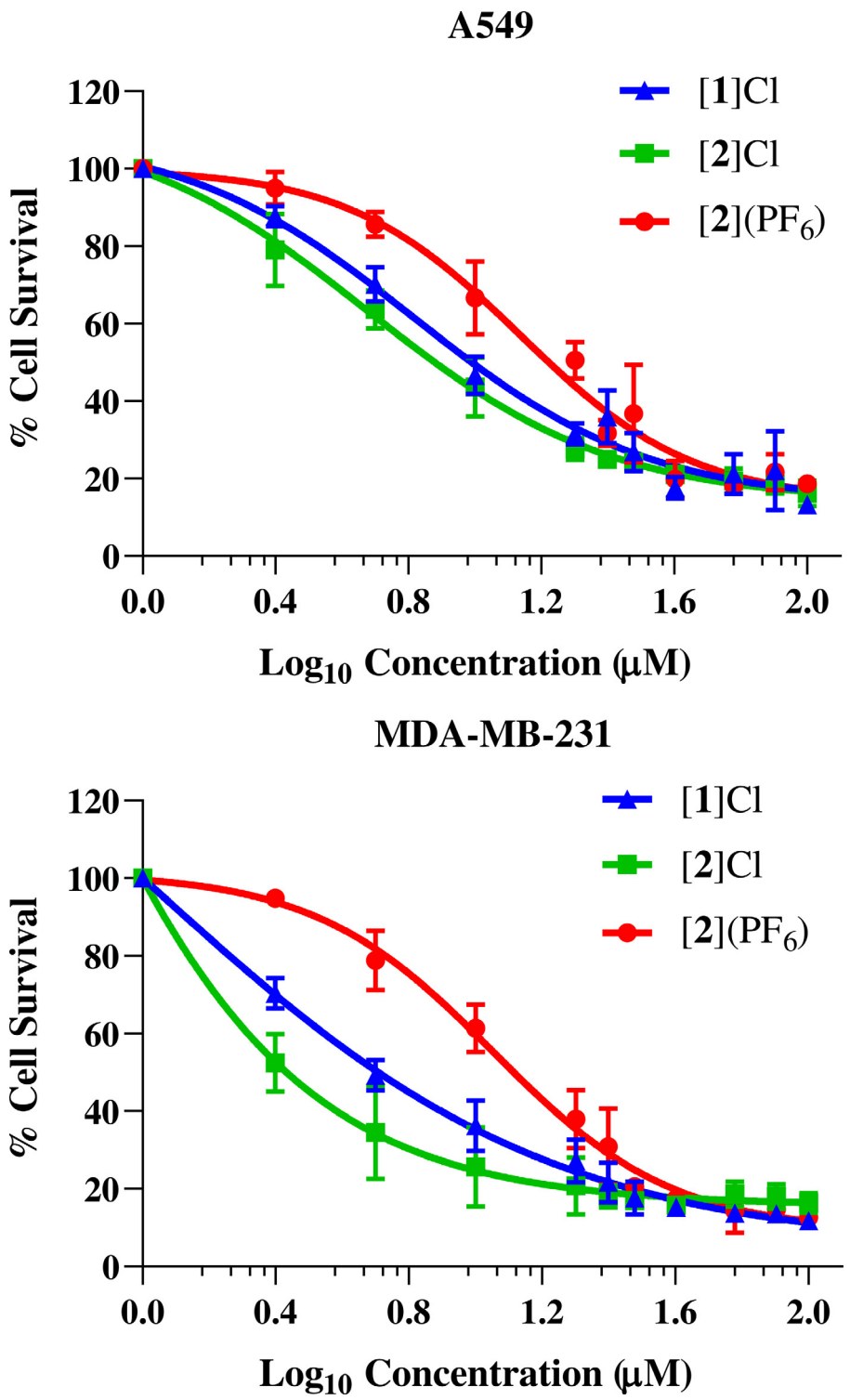

Fig. 11. IC_{50} values showing effect of treatment of [1]Cl, [2]Cl and [2](PF_6) on A549 lung adenocarcinoma and MDA-MB-231 breast adenocarcinoma cells.

tions are longer (distance 3.920 Å) (Figs. S13 and S14). The crystal packing along with hydrogen bonding in the crystal structures of [**2**]Cl and [**2**](PF_6) are given in Supporting Information (Fig. S15).

3.5. Live-cell imaging

Cell cytotoxicity of ruthenium(II) arene complexes were determined in A549; lung adenocarcinoma and MDA-MB-231; breast adenocarcinoma cells. The cells were treated with multiple concentrations of all of them for 72 h. Treatment of A549 and MDA-MB-231 cells with [**1**]Cl, [**2**]Cl and [**2**](PF_6) result in significant cytotoxicity (Figs. 9 and 10). Significant cell death was not observed when the cells were treated with ruthenium(II) complexes for 24 h while moderate death was observed upon treatment for 48 h (Figs. S16–S19). Additionally, consistent cell death was observed upon crystal violet staining of the A549 cells treated with [**1**]Cl, [**2**]Cl and [**2**](PF_6) (Figs. S20 and S21). These observations suggest that the ruthenium complexes are highly efficient in killing cancer cells.

Table 2
Selected bond length (Å) and bond angles (°) for [2]Cl and [2](PF_6)

Bond length / Bond angle	[2]Cl	[2](PF_6)
Ru1–Cl1	2.4011(7)	2.3968(8)
Ru1–N1	2.135(2)	2.119(2)
Ru1–N2	2.062(2)	2.057(2)
Ru1–C2	2.189(3)	2.193(3)
Ru1–C3	2.189(3)	2.161(3)
Ru1–C4	2.196(3)	2.169(3)
Ru1–C5	2.209(3)	2.218(3)
Ru1–C6	2.201(3)	2.200(3)
Ru1–C7	2.170(3)	2.168(3)
N1–Ru1–N2	75.84(8)	76.03(9)
N1–Ru1–Cl1	86.24(6)	84.75(7)
N1–Ru1–C2	119.37(10)	115.01(11)
N1–Ru1–C3	156.55(11)	150.93(12)
N1–Ru1–C4	159.50(10)	166.39(11)
N1–Ru1–C5	121.84(9)	128.38(12)
N1–Ru1–C6	96.86(9)	101.44(11)
N1–Ru1–C7	95.32(10)	95.29(11)
N2–Ru1–Cl1	85.22(7)	82.64(7)
N2–Ru1–C2	92.53(10)	95.65(11)
N2–Ru1–C3	96.80(10)	93.79(11)
N2–Ru1–C4	124.21(10)	117.23(11)
N2–Ru1–C5	162.02(10)	154.17(12)
N2–Ru1–C6	153.30(10)	161.61(12)
N2–Ru1–C7	116.21(10)	123.89(12)

3.6. Cell cytotoxicity in A549 and MDA-MB-231 cells

A colorimetric MTT assay was performed to examine the cytotoxicity induced by ruthenium complexes in A549 lung adenocarcinoma and MDA-MB-231 breast adenocarcinoma cells. The assay was performed using a yellow-colored MTT reagent which gets converted to formazan crystals in live-cells. These crystals were readily dissolved in an acidified isopropanol solvent to give a violet-colored complex which was measured at 595 nm. This conversion takes place in mitochondria and hence the assay determines the viability of cells. We have examined the viability of cancer cells upon treatment of all the complexes after 72 h. The A549 cells treated with [**1**]Cl, [**2**]Cl and [**2**](PF_6) exhibited substantial cell cytotoxicity with IC_{50} values of 6.56 ± 0.31 μM, 4.74 ± 0.2 μM and 13.67 ± 0.64, respectively. Moreover, these complexes showed remarkable cell growth inhibition of MDA-MB-231 cells with an IC_{50} values of 1.13 ± 0.046 μM, 0.36 ± 0.016 μM and 11.32 ± 0.49 μM for [**1**]Cl, [**2**]Cl and [**2**](PF_6) respectively (Fig. 11). No considerable cell death was observed when the cells were treated with all the complexes for 24 h. A549 cells treated with [**1**]Cl, [**2**]Cl and [**2**](PF_6) for 48 h demonstrated cell cytotoxicity with IC_{50} values of 29.7 ± 1.05 μM, 23.5 ± 1.047 μM and 75.6 ± 3.78 μM respectively (Fig. S22). On the other hand, MDA-MB-231 cells exhibited significant cell cytotoxicity with IC_{50} values of 15.99 ± 0.7044 μM, 9.415 ± 0.406 μM and 56.885 ± 1.064 μM when treated with [**1**]Cl, [**2**]Cl and [**2**](PF_6) for 48 h (Fig. S23). Chelopo *et. al.* had demonstrated the anti-tumorigenic property of various ruthenium(II) complexes in several human cancer cell lines including A549 and MDA-MB-231, and observed lowest IC_{50} value of 34 μM after 42 h treatment [48]. Thus, our results demonstrate that [**1**]Cl, [**2**]Cl and [**2**](PF_6) induce remarkable death in cancer cells in a time-dependent manner.

4. Conclusion

In summary, we have successfully explored the versatile half-sandwich ruthenium(II) *p*-cymene complexes comprising substituted triazole ligands and their coordination properties towards promising anticancer agents. The ligands and their corresponding metal complexes have been successfully synthesized and characterized by different spectral and analytical tools. Both the pyrrole substituted ruthenium complexes [**2**]Cl and [**2**](PF_6) have been structurally elucidated by single-crystal X-ray diffraction studies and authenticated the successful anion exchange. The electrochemical study exhibits the non-innocent nature of the targeted metal complexes and ligands. Cellular staining, live-cell imaging and MTT assay have shown remarkable cell cytotoxic effects of [**1**]Cl, [**2**]Cl and [**2**](PF_6) in A549 and MDA-MB-231 cells, ascertaining the anti-oncogenic properties of ruthenium(II) *p*-cymene complexes. Our designed complexes show remarkably better efficacy towards killing cancer cells compared to earlier reported analogous ruthenium(II) *p*-cymene derivatives. Overall, our study provides insights into the role of ligand design of ruthenium(II) *p*-cymene complexes for the development of potential chemotherapeutic agents for the treatment of cancer. This will significantly advance the understanding about the structure-activity relationship to help in the future efficient design of anticancer agents.

Declaration of Competing Interest

The authors declare that they have no known competing financial interests or personal relationships that could have appeared to influence the work reported in this paper.

Acknowledgment

Financial support received from Science and Engineering Research Board (SERB), Department of Science and Technology, India: project no. ECR/2016/000382 (fellowship to S.K.); Council of Scientific and Industrial Research (CSIR) (fellowship to A.M., K.S., B.G. and R.R.) and Indian Institute of Technology Hyderabad are gratefully acknowledged. P.G. acknowledges fellowship support from Ministry of Education. A.M. acknowledges funding support from DST SERB (ECR/2017/002544) and IIT Hyderabad.

Supplementary materials

Supplementary material associated with this article can be found, in the online version, at doi:10.1016/j.jorganchem.2021.122074.

References

[1] M. Waring, B.A. Ponder (Eds.), The Search for New Anticancer Drugs, Springer, Netherlands, 1992.
[2] P. Anand, A.B. Kunnumakara, C. Sundaram, K.B. Harikumar, S.T. Tharakan, O.S. Lai, B. Sung, B.B. Aggarwal, Cancer is a preventable disease that requires major lifestyle changes, Pharm. Res. 25 (2008) 2097.
[3] L. Falzone, S. Salomone, M. Libra, Evolution of cancer pharmacological treatments at the turn of the third millennium, Front. Pharmacol. 9 (2018) 1300.
[4] M. Arruebo, N. Vilaboa, B. Sáez-Gutierrez, J. Lambea, A. Tres, M. Valladares, Á. González-Fernández, Assessment of the evolution of cancer treatment therapies, Cancers (Basel) 3 (2011) 3279–3330.
[5] C. Pucci, C. Martinelli, G. Ciofani, Innovative approaches for cancer treatment: current perspectives and new challenges, E. Cancer Med. Sci. 13 (2019) 961.
[6] S. Dilruba, G.V. Kalayda, Platinum-based drugs: past, present and future, Cancer Chemother. Pharmacol. 77 (2016) 1103–1124.
[7] J. Zhou, Y. Kang, L. Chen, H. Wang, J. Liu, S. Zeng, L. Yu, The drug-resistance mechanisms of five platinum-based antitumor agents, Front. Pharmacol. 11 (2020).
[8] Anticancer agents beyond cisplatin, in: Metals in Medicine, John Wiley & Sons, Ltd, 2017, pp. 157–216.
[9] B.J. Reedijk, Metal-ligand exchange kinetics in platinum and ruthenium complexes, Platinum Met. Rev. 52 (2008) 2–11.
[10] C. Moucheron, From cisplatin to photoreactive Ru complexes: targeting DNA for biomedical applications, New J. Chem. 33 (2009) 235–245.
[11] G. Süss-Fink, Arene ruthenium complexes as anticancer agents, Dalton Trans. 39 (2010) 1673–1688.
[12] M.R. Gill, J.A. Thomas, Ruthenium(II) polypyridyl complexes and DNA—from structural probes to cellular imaging and therapeutics, Chem. Soc. Rev. 41 (2012) 3179–3192.

[13] B. Giri, T. Saini, S. Kumbhakar, K K.S., A. Muley, A. Misra, S. Maji, Near-IR light-induced photo release of nitric oxide (NO) on ruthenium nitrosyl complexes: formation, reactivity, and biological effects, Dalton Trans 49 (2020) 10772–10785.
[14] A. Casini, C. Gabbiani, F. Sorrentino, M.P. Rigobello, A. Bindoli, T.J. Geldbach, A. Marrone, N. Re, C.G. Hartinger, P.J. Dyson, L. Messori, Emerging protein targets for anticancer metallodrugs: inhibition of thioredoxin reductase and Cathepsin B by antitumor ruthenium(II)–arene compounds, J. Med. Chem. 51 (2008) 6773–6781.
[15] M.P. Chelopo, S.A. Pawar, M.K. Sokhela, T. Govender, H.G. Kruger, G.E.M. Maguire, Anticancer activity of ruthenium(II) arene complexes bearing 1,2,3,4-tetrahydroisoquinoline amino alcohol ligands, Eur. J. Med. Chem. 66 (2013) 407–414.
[16] M.J. Chow, C. Licona, D. Yuan Qiang Wong, G. Pastorin, C. Gaiddon, W.H. Ang, Discovery and investigation of anticancer ruthenium–Arene Schiff-base complexes via water-promoted combinatorial three-component assembly, J. Med. Chem. 57 (2014) 6043–6059.
[17] C.M. Clavel, E. Păunescu, P. Nowak-Sliwinska, A.W. Griffioen, R. Scopelliti, P.J. Dyson, Modulating the anticancer activity of ruthenium(II)–arene complexes, J. Med. Chem. 58 (2015) 3356–3365.
[18] F. Wang, H. Chen, S. Parsons, I.D.H. Oswald, J.E. Davidson, P.J. Sadler, Kinetics of aquation and anation of ruthenium(II) arene anticancer complexes, acidity and X-ray structures of aqua adducts, Chem. Eur. J. 9 (2003) 5810–5820.
[19] P. Crochet, V. Cadierno, Arene-ruthenium(II) complexes with hydrophilic P–donor ligands: versatile catalysts in aqueous media, Dalton Trans. 43 (2014) 12447–12462.
[20] A. Habtemariam, M. Melchart, R. Fernández, S. Parsons, I.D.H. Oswald, A. Parkin, F.P.A. Fabbiani, J.E. Davidson, A. Dawson, R.E. Aird, D.I. Jodrell, P.J. Sadler, Structure–activity relationships for cytotoxic ruthenium(II) arene complexes containing N,N-, N,O-, and O,O- chelating ligands, J. Med. Chem. 49 (2006) 6858–6868.
[21] M.J. Chow, C. Licona, G. Pastorin, G. Mellitzer, W.H. Ang, C. Gaiddon, Structural tuning of organoruthenium compounds allows oxidative switch to control ER stress pathways and bypass multidrug resistance, Chem. Sci. 7 (2016) 4117–4124.
[22] S. Betanzos-Lara, L. Salassa, A. Habtemariam, O. Novakova, A.M. Pizarro, G.J. Clarkson, B. Liskova, V. Brabec, P.J. Sadler, Photo activatable organometallic pyridyl ruthenium(II) arene complexes, Organometallics 31 (2012) 3466–3479.
[23] G.S. Yellol, A. Donaire, J.G. Yellol, V. Vasylyeva, C. Janiak, J. Ruiz, On the antitumor properties of novel cyclometalated benzimidazole Ru(II), Ir(III) and Rh(III) complexes, Chem. Commun. 49 (2013) 11533–11535.
[24] J. Yellol, S.A. Pérez, A. Buceta, G. Yellol, A. Donaire, P. Szumlas, P.J. Bednarski, G. Makhloufi, C. Janiak, A. Espinosa, J. Ruiz, Novel C,N-cyclometalated benzimidazole Ruthenium(II) and Iridium(III) complexes as antitumor and antiangiogenic agents: a structure–activity relationship study, J. Med. Chem. 58 (2015) 7310–7327.
[25] R. Pettinari, F. Marchetti, F. Condello, C. Pettinari, G. Lupidi, R. Scopelliti, S. Mukhopadhyay, T. Riedel, P.J. Dyson, Ruthenium(II)–arene RAPTA type complexes containing curcumin and bisdemethoxycurcumin display potent and selective anticancer activity, Organometallics 33 (2014) 3709–3715.
[26] C.S. Allardyce, P.J. Dyson, D.J. Ellis, S.L. Heath, [Ru(η^6-*p*-cymene)Cl_2(pta)] (pta = 1,3,5-triaza-7-phosphatricyclo-[3.3.1.1]decane): a water soluble compound that exhibits pH dependent DNA binding providing selectivity for diseased cells, Chem. Commun. (2001) 1396–1397.
[27] C. Scolaro, A. Bergamo, L. Brescacin, R. Delfino, M. Cocchietto, G. Laurenczy, T.J. Geldbach, G. Sava, P.J. Dyson, In vitro and in vivo evaluation of Ruthenium(II)–arene PTA complexes, J. Med. Chem. 48 (2005) 4161–4171.
[28] A. Bergamo, A. Masi, P.J. Dyson, G. Sava, Modulation of the metastatic progression of breast cancer with an organometallic ruthenium compound, Int. J. Oncol. 33 (2008) 1281–1289.
[29] A. Weiss, R.H. Berndsen, M. Dubois, C. Müller, R. Schibli, A.W. Griffioen, P.J. Dyson, P. Nowak-Sliwinska, In vivo anti-tumor activity of the organometallic ruthenium(II)-arene complex [Ru(η^6-*p*-cymene)Cl_2(pta)] (RAPTA-C) in human ovarian and colorectal carcinomas, Chem. Sci. 5 (2014) 4742–4748.
[30] F. Linares, M.A. Galindo, S. Galli, M.A. Romero, J.A.R. Navarro, E. Barea, Tetra-nuclear coordination assemblies based on half-sandwich ruthenium(II) complexes: non-covalent binding to DNA and cytotoxicity, Inorg. Chem. 48 (2009) 7413–7420.
[31] A. Mishra, S.C. Kang, K.-W. Chi, Coordination-driven self-assembly of arene–ruthenium compounds, Eur. J. Inorg. Chem. 2013 (2013) 5222–5232.
[32] A.K. Singh, D.S. Pandey, Q. Xu, P. Braunstein, Recent advances in supra-molecular and biological aspects of arene ruthenium(II) complexes, Coord. Chem. Rev. 270–271 (2014) 31–56.
[33] B. Therrien, Biologically relevant arene ruthenium metalla-assemblies, CrystEngComm 17 (2014) 484–491.
[34] F. Schmitt, J. Freudenreich, N.P.E. Barry, L. Juillerat-Jeanneret, G. Süss-Fink, B. Therrien, Organometallic cages as vehicles for intracellular release of photosensitizers, J. Am. Chem. Soc. 134 (2012) 754–757.
[35] M.A. Bennett, T.-N. Huang, T.W. Matheson, A.K. Smith, S. Ittel, W. Nickerson, in: 16. (η^6-Hexamethylbenzene)Ruthenium Complexes, in: Inorganic Syntheses, John Wiley & Sons, Ltd, 1982, pp. 74–78.
[36] M.H. Klingele, P.D.W. Boyd, B. Moubaraki, K.S. Murray, S. Brooker, Probing the dinucleating behavior of a bis-bidentate ligand: Synthesis and characterization of some di- and mononuclear cobalt(II), nickel(II), copper(II) and zinc(II) complexes of 3,5-di(2-pyridyl)-4-(1H-pyrrol-1-yl)-4H-1,2,4-triazole, Eur. J. Inorg. Chem. 2006 (2006) 573–589.
[37] G.M. Sheldrick, A short history of SHELX, Acta Cryst. A 64 (2008) 112–122.
[38] G.M. Sheldrick, Crystal structure refinement with SHELXL, Acta Cryst. C. 71 (2015) 3–8.
[39] V.J. Catalano, T.J. Craig, Synthesis and X-ray crystal structures of several dinuclear ruthenium cymene complexes based on the tetradentate ligand, 2,2′-(1H-pyrazole-3,5-diyl)bis(6-methylpyridine) (Me_2DppzH), Polyhedron 19 (2000) 475–485.
[40] G. Gupta, G.P.A. Yap, B. Therrien, K.Mohan Rao, Study of novel η^5-cyclopentadienyl and η^6-arene platinum group metal complexes containing a N4-type ligand and their structural characterization, Polyhedron 28 (2009) 844–850.
[41] A. Singh, N. Singh, D.S. Pandey, Stable mononuclear and binuclear ruthenium(II) arene complexes with multiple N-donor poly-pyridyl ligands: synthesis, spectroscopic and structural characterization. Single crystal X-ray structure of [(η^6-$C_{10}H_{14}$)RuCl(bppz)]BF_4, J. Organomet. Chem. 642 (2002) 48–57.
[42] B. Giri, S. Kumbhakar, K. Kalai Selvan, A. Muley, S. Maji, Formation, reactivity, photo release, and scavenging of NO in ruthenium nitrosyl complexes, Inorg. Chim. Acta. 502 (2020) 119360.
[43] B. Giri, S. Kumbhakar, K.S. K, A. Muley, S. Maji, Ruthenium nitrosyl complexes with the molecular framework [Ru^{II}(dmdptz)(bpy)(NO)]$^{n+}$ (dmdptz: N,N-dimethyl-4,6-di(pyridin-2-yl)-1,3,5-triazin-2-amine and bpy: 2,2′-bipyridine). Electronic structure, reactivity aspects, photo release, and scavenging of NO, New J. Chem. 44 (2020) 18732–18744.
[44] S. Maji, B. Sarkar, S. Patra, J. Fiedler, S.M. Mobin, V.G. Puranik, W. Kaim, G.K. Lahiri, Metal-induced reductive ring opening of 1,2,4,5-Tetrazines: three resulting coordination alternatives, including the new non-innocent 1,2-diiminohydrazido(2−) bridging ligand system, Inorg. Chem. 45 (2006) 1316–1325.
[45] D. Kumbhakar, B. Sarkar, S. Maji, S.M. Mobin, J. Fiedler, F.A. Urbanos, R. Jiménez-Aparicio, W. Kaim, G.K. Lahiri, Intra-molecular valence and spin interaction in meso and rac diastereomers of a *p*-quinonoid-bridged diruthenium complex, J. Am. Chem. Soc. 130 (2008) 17575–17583.
[46] N. Busto, M. Martínez-Alonso, J.M. Leal, A.M. Rodríguez, F. Domínguez, M.I. Acuña, G. Espino, B. García, Monomer–dimer divergent behavior toward DNA in a half-sandwich ruthenium(II) aqua complex. anti-proliferative biphasic activity, Organometallics 34 (2015) 319–327.
[47] K. Salzmann, C. Segarra, M. Albrecht, Donor-flexible bis(pyridylidene amide) ligands for highly efficient ruthenium-catalyzed olefin oxidation, Angew. Chem. Int. Ed. 59 (2020) 8932–8936.
[48] M.P. Chelopo, S.A. Pawar, M.K. Sokhela, T. Govender, H.G. Kruger, G.E.M. Maguire, Anticancer activity of ruthenium(II) arene complexes bearing 1,2,3,4-tetrahydroisoquinoline amino alcohol ligands, Eur. J. Med. Chem. 66 (2013) 407–414.